ARITHMETIC METHODS
IN MATHEMATICAL PHYSICS AND BIOLOGY
BANACH CENTER PUBLICATIONS, VOLUME 109
INSTITUTE OF MATHEMATICS
POLISH ACADEMY OF SCIENCES
WARSZAWA 2016

THE CIRCULAR FRACTAL MODEL OF ADENOCARCINOMAS AND TUMOR AGGRESSIVENESS

PRZEMYSŁAW WALISZEWSKI

Department of Urology, Pediatric Urology and Andrology, Justus-Liebig University
Rudolf-Buchheim-Strasse 7, 35392 Giessen, Germany
E-mail: complexityresearch@yahoo.com

Abstract. There is no golden standard for the evaluation of tumor aggressiveness in pathology. This results in a high inaccuracy of both tumor grading and assessment of the progression risk as well as in unnecessary treatment of patients. Using some histological features of adenocarcinomas, a universal approach based on the circular fractal geometrical model and three global fractal dimensions of the Rényi family as the complexity measures of the spatial distribution of cancer cell nuclei in adenocarcinomas is proposed. This model is both geometrical and analytical. It can be used to select and calibrate the software for the image analysis. Both the global fractal dimension D_0 and the global information dimension D_1 allow the objective stratification of carcinomas into the classes of equivalence. The correlation coefficient between those two dimensions is about 0.95. The mean value of the global capacity fractal dimension D_0 1.5820 defines a limit between low-grade prostate carcinomas with a well-preserved glandular structure and high-grade prostate carcinomas with more altered spatial distribution of cancer cell nuclei. This model has been validated by analyzing a large set of prostate carcinomas. According to the Bekenstein Bound, the amount of information present in the finite fractals representing the idealized distribution of cancer cell nuclei is limited, and changes linearly as 1 : 1.94 : 2.64. A similar relationship can be seen in changes of entropy S in a function of the D_0. Entropy also increases in a linear manner with the coefficient of correlation 0.904 and, therefore, determines the natural course of disease. Finally, the circular fractals $\mathrm{CF}(6+0)$ and $\mathrm{CF}(6+1)$ have the same topology. This means that the corresponding patterns of growth, albeit with different histological structure, are generated by the same dynamic forces, and may reveal the same aggressiveness. Therefore, they should be classified in the high-risk category. This novel, objective approach enables a stratification of prostate carcinomas into a category of low, intermediate or high aggressiveness. The subjective tumor grading should also be simplified.

2010 *Mathematics Subject Classification*: Primary 92B99; Secondary 92-08.
Key words and phrases: circular fractals, global fractal dimension, topology, fractal image analysis, tumor grading, tumor aggressiveness, prostate, carcinoma, digital pathology, histology.
The paper is in final form and no version of it will be published elsewhere.

DOI: 10.4064/bc109-0-12

1. Introduction. Tissue growth is a fundamental biological phenomenon that occurs simultaneously in both time and space [26, 24]. It comprises such processes as proliferation of cells, i.e., multiplication of a cell number, and maturation, i.e., modification of cell size, regulation of metabolism, expression of some tissue-specific proteins, or activation of some specialized functions by cells until the final cell phenotype emerges. Finally, cells self-organize into tissue structures of the higher order, such as glands, rosettes, or clusters. This is a characteristic spatial imprint of the dynamic temporal-spatial phenomena of growth and self-organization resulting from the multitude of intercellular interactions between epithelial cells and mesenchymal stroma [11]. Diverse molecular signaling pathways cooperate in the initiation and progression of the epithelial-mesenchymal transition and mesenchymal-epithelial transition. This occurs through regulation at transcriptional, post-transcriptional, translational, and post-translational levels [15]. The strength of those interactions can be best exemplified by the morphological and molecular changes that occur in populations of malignant prostate epithelial cells growing in different microenvironments, such as in vitro culture or embryos [5].

Malignant cells follow the same route to some extent. They can also form tissue structures of the higher order. If we know the typical features of normal cells and normal tissue architecture, it is possible to compare both tissues, and determine a degree of histological similarity. This degree of similarity is known as tumor grading. Grading systems differ in details depending on the type of malignancy. In the case of carcinomas, that is, malignant tumors of epithelial origin, tumor structure is usually graded as 1, 2, 3, or 4, depending on the degree of dissimilarity with the normal tissue. In the case of grade 1 well-differentiated carcinomas, malignant cells and their organization in glands appear to be close to normal. Those carcinomas tend to grow slowly and metastasize infrequently. Intermediate-differentiated carcinomas of grade 2, poor-differentiated carcinomas of grade 3 or non-differentiated carcinomas of grade 4 have cells or glands with more and more altered appearance. Non-differentiated carcinomas of grade 4 do not look like any normal counterpart, and, sometimes, their origin cannot be determined unequivocally. Those carcinomas grow rapidly and spread to lymph nodes or blood vessels faster than carcinomas with the lower grades.

In the case of prostate carcinomas, forty different grading systems were proposed (reviewed in [12]). However, a system of grading according to Gleason criteria with at least seven grades is used most frequently [9, 18]. Prostate carcinomas are known for their tremendous morphological variability. According to the Gleason system, pathologists identify two, or sometimes even three, most frequent patterns of cellular organization. The primary pattern is the most common pattern of cell organization seen in the particular carcinoma, and the secondary pattern represents the next most common pattern, etc. In the first version of the Gleason system, each pattern was given a grade from 1 to 5, with 1 looking the most like normal prostate tissue and 5 looking the most abnormal. In the version of 2010, the grade 1 and 2 were eliminated because, except of biopsies, they were never seen in the surgical prostate specimen. In addition, pathologists attempt to evaluate a percentage of the tumor surface occupied by the given pattern. The two most frequent grades are then added to give a Gleason score [7, 6]. For example, 70% of the

image surface occupied by the well-preserved glands of different sizes co-existing with pseudoglands (20%), and with cellular infiltrates (10%) produces the following Gleason score $3 + 4 + (5)$.

A study of natural history of different malignancies since the time of Virchow showed that the more altered tumor tissue architecture the more aggressive behavior of malignant cells and the greater their metastatic potential [8]. In this way, the subjective tumor grading became a measure of tumor aggressiveness; the most important parameter for the evaluation of tumor growth in space [10]. Unfortunately, both the lack of a golden pattern and standardization cause that the subjective evaluation of tumor aggressiveness has a significant inter- and intraobserver variability. For prostate adenocarcinomas, this variability is about 40%–80% [7, 6, 20]. This variability influences the accuracy of the risk assessment of tumor progression in any statistical model based on tumor grading, such as Kattan nomograms [13], which is about 70%. A comparison of results between different patients or clinical centers is in this situation difficult, and has a limited reliability.

To deal with this problem, a number of experimental approaches was proposed. First, some comparative studies at the DNA, RNA, protein or organ level (MRI techniques) were conducted [3, 16, 17, 21, 23]. As might be expected, a correlation coefficient between the subjective tumor grading according to Gleason and the proposed biomarkers was rather low, in the range of 0.1–0.6. Assuming that a combination of clinical information and genetic one should yield clinical information with genetic information should yield better outcome predictions, two gene kits, the Oncotype DX one, examining the expression of 17 aggressive tumor-predictive genes in biopsy specimen [14] or the Myriad Prolaris Assay that examines the expression of 31 such genes [4] were offered recently. The future clinical studies will show if those kits do generate better prediction accuracy. Also, prostate MRI study remains nonspecific and biopsies must be performed anyway to confirm a cancer diagnosis and to evaluate tumor aggressiveness.

The reduction of inter- and intraobserver variability may occur in two ways. First, the histological evaluation of tumor aggressiveness can be done in the hierarchical system of pathologists known as a central register [19]. Second, the grading system could be simplified in such a manner that pathologist would define only two categories of carcinomas. The first one would be a category of carcinomas with a very well-preserved glandular structure predestinating patients to active surveillance. The second category would comprise carcinomas with more severe morphological alterations subject to immediate aggressive treatment. In the case of prostate cancer, this is one out of three pieces of information, besides PSA concentration and pTNM staging, that are relevant to the clinicians in order to make a decision: to treat or not to treat?

The elimination of that variability is possible only then, if pathologists get some supportive tools for computer image analysis. Those tools can generate the objective, quantitative measures characterizing patterns of tumor growth in space. Since there is no golden pattern in tumor pathology, a circular fractal model of prostate adenocarcinomas is proposed. This model is both geometrical and analytical. It is based on some characteristic features of the prostate adenocarcinoma structure, and allows a calculation of the values of the global fractal dimensions. In fact, that model seems to be universal enough to describe patterns of growth of any adenocarcinomas independent of tissue of origin. The goal of

this study is to validate both the model for prostate adenocarcinomas and the resulting classes of equivalence as well as to justify the reduction of the number of grades used in the subjective Gleason system.

2. A circular fractal model of adenocarcinomas. The fundamental idea of fractal geometry is to assume that the geometric variables, i.e., length, surface or volume and scale (reduction factor) do not vary arbitrarily but rather are related by a power law, in which the spatial fractal dimension is a coefficient, i.e., a power index of non-integer value relating scale and the number of pieces into which the entire structure can be divided during the similarity transformation.

Cancer cell nuclei can be easily identified by the specialized computer algorithms in the digitalized image of tumor tissue owing to both strong contrast and differences in nuclei shape of various cell types. From the geometrical perspective, a set of cancer cell nuclei is the set of the fragments of surface with the dimension 2.0 rather than the set of points with the dimension zero. Since that set undergoes some self-similar or self-affine transformation during tumor progression, one can expect that the distribution of cancer cell nuclei should possess structure of the finite stochastic fractal or multifractal, that is, fractals that scale with multiple scaling rules and $D_0 > D_1 > D_2$. This structure will be characterized well by the global fractal dimensions with the mean values greater than 1.0 and lower than 2.0.

The idealized geometric model mimics the basic patterns of growth seen in natural history of adenocarcinomas. The cornerstone of the approach is a model composed of the circular fractals CF(3) or CF(4), CF(6+0), and CF(6+1). This model is both geometrical and analytical, i.e., its structure is well-defined, the capacity fractal dimension D_0 can be calculated for the infinite circular fractals, and the dimensions D_0, D_1, D_2 can be computed for their finite counterparts representing distribution of cell nuclei. The model enables a computation of the global fractal dimensions to be expected for the distribution of cell nuclei in a given carcinoma subtype, and, therefore, may serve as a frame of reference for a validation of the results of computation for the real images of carcinomas. In the case of adenocarcinomas with well-preserved, irregular and branched glands of different sizes, such as those in prostate adenocarcinomas with the Gleason score $3 + 3$, cell nuclei, sparsely distributed along the gland outline, are several-fold smaller than glands (see Figure 1A and 1D). There are no infiltrating cancer cells. The geometric relationship of that pattern represents the circular fractal CF(3) or CF(4) (not shown in Figure 1), in which circles of different sizes and colors corresponding to the consecutive iterations depict a variety of gland sizes. Adenocarcinomas with small, regular, circle-like glands and with a component of cell infiltration are represented in the model by the circular fractal CF$(6 + 0)$. This fractal represents a prostate carcinoma pattern with the Gleason score $4 + 4$.

The circular fractal CF$(6 + 1)$ represents carcinoma architecture, such as this seen in prostate carcinomas with the Gleason score $5 + 5$. This pattern is defined as a disordered cell infiltration without gland-like structures. The black dots that mimic cell nuclei cover almost the entire surface and leave a minimal amount of free space [25] (see Figure 1).

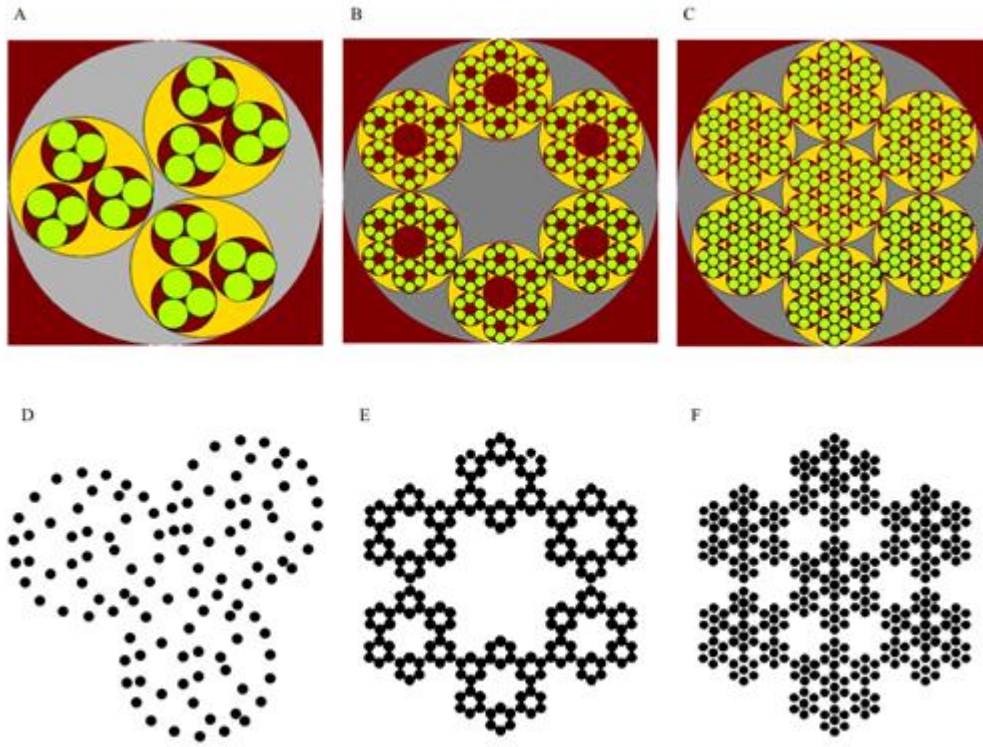

Figure 1. A universal, simplified and idealized model of the patterns of growth seen in natural history of adenocarcinomas. The surface is covered by a set of the two-dimensional fragments mimicking cell nuclei in such a manner that they reflect some geometrical features seen in the real images of carcinomas. The circular fractal model is both geometrical and analytical. It plays a role of the frame of reference during a choice of the software and its calibration. The model enables prediction of the expected mean values of the global fractal dimensions of the Rényi family, D_0, D_1, and D_2 for each pattern. Also, complexity of those systems can be calculated and compared by using the Bekenstein Bound (Limit) formula. Finally, the identical topology suggests the same dynamic forces operate in the case of the patterns depicted in 1E and 1F. Therefore, both patterns represent, despite some structural differences, carcinomas of the same high-grade; a conclusion confirmed by the amount of information according to Bekenstein and the changes of entropy S in a function of the D_0. There are shown three iterations of the infinite circular fractal CF(3) (A), CF($6 + 0$) (B), and CF($6 + 1$) (C), representing the spatial distribution of cancer cells nuclei in tumor architecture typical for the Gleason grade 3, 4, or 5, respectively. The model based on those three circular fractals reflects some geometrical features of (A) well-differentiated adenocarcinomas with the Gleason score $3 + 3 = 6$, characterized by regular, circle-like glands of different sizes, and cancer cell nuclei much smaller than the size of glands as shown on Figure 1D; (B) intermediate-differentiated ones with the Gleason-score $4 + 4 = 8$, having multiple regular, small pseudoglands composed of clusters of a few cancer cells, and (C) poor-differentiated ones with the Gleason score $5 + 5 = 10$ with malignant cell infiltrates filling almost the entire tissue space. A single iteration of those fractals shown in D, E, and F depicts both the spatial distribution of cell nuclei and their size in relationship to the size of glands.

The geometrical model predicts the following values of the capacity fractal dimension D_0: $D_0 < 1.573$ for the pattern with the Gleason score $3 + 3 = 6$ or for well-differentiated carcinomas G1 (see Figure 1A and 1D), $1.631 < D_0 < 1.771$ for the pattern with the Gleason score $4 + 4$ or for intermediate-differentiated carcinomas G2 (Figure 1B and 1E), $D_0 > 1.771$ for the pattern with the Gleason score $5+5$ or for poor-differentiated carcinomas G3 (Figure 1C and 1F) [25].

The following values of the global fractal dimensions D_0 and D_1 were computed from the model images of the finite circular fractals with the number of iterations limited to the nuclei level of the size 648×432 pixels: CF(3) 1.515 (021), 1.514 (019); CF(4) 1.520 (082), 1.522 (030); CF(6+0) 1.642 (009), 1.672 (004); CF(6+1) 1.712 (004), 1.754 (001), respectively. The values of D_2 generated by the software Fractalyse were as follows: CF(3) 1.521 (009); CF(4) 1.584 (021); CF(6 + 0) 1.701 (011); CF(6 + 1) 1.788 (026).

3. A validation of the circular fractal model. This study was performed according to the ethical standards outlined in the WMA Declaration of Helsinki *Ethical Principles for Medical Research Involving Human Subjects* (http://www.wma.net). Tissues were obtained from the following institutes of pathology: University Medical School, Poznań, Poland (prostate carcinomas), Justus-Liebig University, Giessen, Germany (prostate adenomas and carcinomas), Fichtelgebirge Klinikum, Marktredwitz, Germany (prostate carcinomas). Tissues were stained with hematoxylin and eosin. In the case of prostate carcinomas, the additional immunohistochemical stainings with the appropriate antibodies against the markers, i.e., PSA (DAKO, Germany) and AMACR (DAKO, Germany) for prostate cancer cells, cytokeratin 34βE12 (Leica Biosystems, Canada) for basal cells were performed in order to confirm the diagnosis, and to classify those carcinomas by the Gleason criteria. The histological evaluation of the cases was done by teams of pathologists working in the above mentioned institutes.

A set of prostate carcinomas comprising 173 carcinomas with the following Gleason score: $3 + 3 = 6$ ($n = 35$), $3 + 4 = 7a$ ($n = 18$), $4 + 3 = 7b$ ($n = 14$), $4 + 4 = 8$ ($n = 23$), $4 + 5 = 9$ ($n = 28$), $5 + 4 = 9$ ($n = 20$), $5 + 5$ ($n = 35$) and a set of benign prostatic hyperplasia ($n = 20$) were analyzed. None of the patients had lymphatic or distant metastases.

(i) Image digitalization. Histological slides of carcinomas stained with hematoxylin and eosin were digitalized using both a microscope Axioskop 5.0 with the halogen lamp 12V 50W 2800K 950lm and the objective Plan Neofluar 20× with the numerical aperture 0.5, Zeiss, Germany and a camera Nikon Coolscope, Japan. The optimal conditions for the magnification (20×) and lighting intensity ($41.19 \cdot 10^6$ lx) were chosen in such a manner that the values of the capacity fractal dimension for the test image were in the plateau-area of the test curve (data not shown).

The color images in the bmp format with 1240×1000 pixels and resolution 150×150 dpi were first resized to the jpg format with 648×432 pixels and resolution 150×150 dpi. Cancer cell nuclei were isolated electronically using a package Definiens Tissue Map ver. 7.0 (Definiens, Munich, Germany), and stored as RPG images in the jpg format with 648×432 pixels, resolution 150×150 dpi. Both conversion to the 8-bit images

and their thresholding to the binary images, that is, images having only 0 (black) and 255 (white) pixel values was performed using the Rényi Entropy filter of the open-source software Image J ver 1.48v (NIH, Bethesda, USA, http://imagej.nih.gov/ij/).

The images were analyzed by the computer algorithms measuring the global fractal dimensions of the Rényi family, i.e. capacity dimension D_0 and information dimension D_1 (Benoit 1.3, True Soft, USA, http://www.trusoft-international.com/benoit.html), and correlation dimension D_2 (Fractalyse 2.4, CNRS Université de Franche-Comté, France, http://www.fractalyse.org). The values of the global fractal dimensions generated by the computer algorithms were verified against the geometrical model [25]. Entropy was measured using Matlab R2012a and its Image Analysis Toolbox.

(ii) Statistical analysis. The statistical analysis including the ROC analysis was performed by Sigma Plot ver. 10.0 (http://www.sigmaplot.com, Systat Software Inc., San Jose, USA). The following aspects are important while analyzing a ROC curve. The ROC curve is a two dimensional graph. It represents a relationship between sensitivity of a statistical test (y-axis) in a function of 1-specificity of that test (x-axis). Sensitivity is defined as a rate of true positive events. The second quantity represents a rate of non-events that were falsely identified as positive events for the different cut-off values of a binary classifier, such as D_0, D_1 or D_2, etc. Second, the closer the ROC curve follows the y-axis, and then the top border of the ROC diagram, the more accurate the statistical test. The area under the ROC curve (AUC) is a probability of the test accuracy, i.e., a probability that the classifier discriminates between the elements of two sets correctly. The AUC of 1.0 denotes a perfect relationship between the data that belong to a given category and those that do not. Third, the closer the ROC curve comes to the diagonal of the ROC diagram, the AUC is closer to 0.5, which denotes that the test is not able to discriminate between two sets of data. The re-stratification of carcinomas on the basis of the fractal dimensions D_0, D_1, and D_2 into the complexity classes is equivalent to the task of the identification the cut-off values of the best classifier, i.e., the classifier generating the AUC of 1.

(iii) Inaccuracy of the subjective histological evaluation. Subjective evaluation of tumor aggressiveness causes that carcinomas are not classified in the predictable manner. Human eye and mind evaluate pretty well the homogeneous structure, such as well-preserved prostate glands of a similar size (the Gleason score $3+3=6$) or dense cellular infiltrates (the Gleason score $5+5$). However, more complex patterns, such as those in borderline cases with the Gleason score $3+4=7a$, $4+3=7b$, $4+5=9$ or $5+4=9$ are classified with a significant inaccuracy [27] (compare Figure 2). Frequently, it is almost impossible to match the real image to the grade definition. In those cases, regular gland structure mixes with small pseudoglands or with cell infiltrates to different extent. Those details cannot be easily evaluated by eye quantitatively. Yet, a different percentage of cellular infiltrates or small pseudoglands in the images may indicate differences in tumor aggressiveness and, in consequence, a different clinical course of the disease. There is a need for a quantitative and objective system of evaluation of tumor aggressiveness that might be used for a comparison of carcinomas, not only in prostate, but also in adenocarcinomas of the other epithelial tissues.

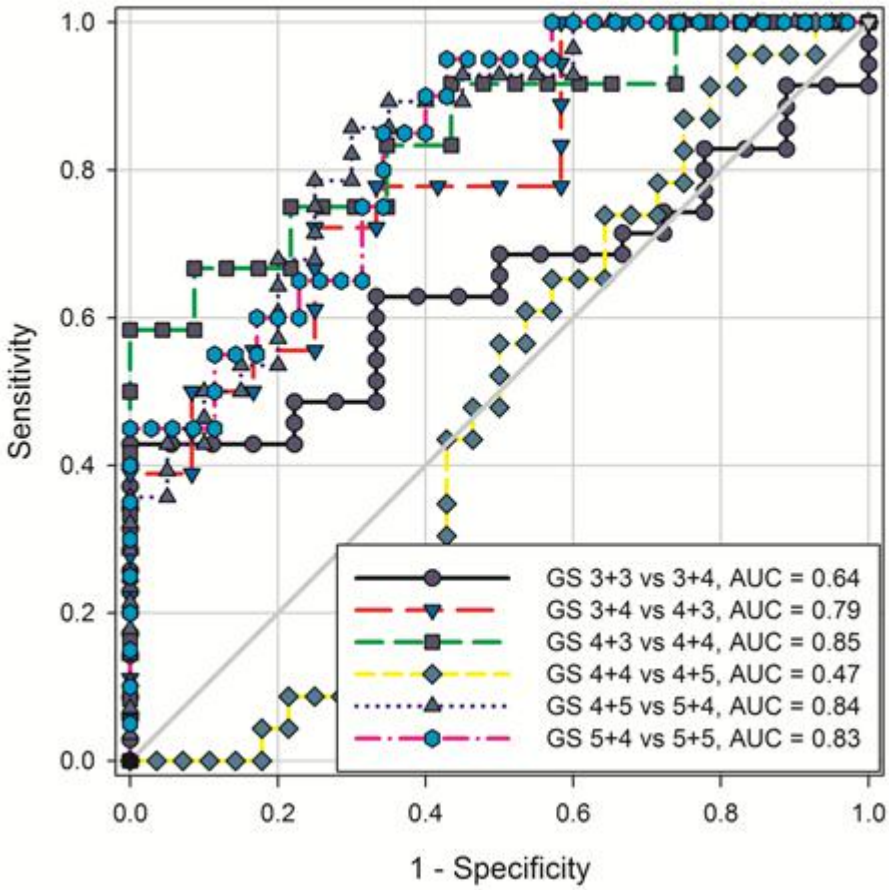

Figure 2. Results of the ROC analysis for the set of 173 prostate adenocarcinomas. In each case, the global fractal capacity dimension D_0 was measured. The subgroups of carcinomas classified according to the Gleason criteria were compared. There is a significant inaccuracy in tumor grading and overlapping between the subgroups as controlled by the values of the D_0. Since the algorithm for the assessment of tumor progression risk is based on three elements: PSA concentration, tumor stage, and tumor grading. Its discriminating power is low, about 70%. GS stands for the Gleason score subjectively ascribed by pathologists during tumor grading, AUC denotes area under curve.

(iv) Classes of equivalence. Measurements of the global fractal dimensions of the Rényi family in the real images with the application of different software based on the same computer algorithms shows that the results are not identical (see Table 1). This software is usually calibrated using very simple geometric objects, such as line, circle, triangle, or square. The results in those simple cases tally with theoretical calculations.

In the case of the complex images, some other factors, such as image positioning, a different number of iterations, a different size of the initial grid, grid rotation, and the way

statistical analysis is performed, that have been defined arbitrarily by the programmers, lead to a discrepancy of the results. Also, a choice of the options within the software may influence the results of image analysis (see Table 1).

Benoit		Fractalyse		Image J	
D_0	D_1	D_0	D_1	D_0	D_1
1.6305	1.6305	1.6673	1.6972	1.7776	1.7519
1.6449	1.6520	1.6498	1.6738	1.7481	1.7244
1.6196	1.6276	1.6224	1.6180	1.7189	1.6857
1.6365	1.6517	1.5972	1.5699	1.6947	1.6496
1.6157	1.6251	1.6039	1.5722	1.6984	1.6441
1.5999	1.6105	1.6710	1.6586	1.7618	1.7302
1.5955	1.6053	1.6257	1.6446	1.7466	1.7151
1.5906	1.6032	1.6021	1.6216	1.7144	1.6878
1.5784	1.5905	1.5845	1.5938	1.6824	1.6528
1.5627	1.5757	1.5481	1.5341	1.6431	1.5978

Table 1. A comparison of the global fractal dimensions D_0 and D_1 obtained by using Benoit, Fractalyse, or Image J software for ten consecutive prostate adenocarcinomas with a well-preserved glandular structure and the subjective Gleason score $3+4=7a$. Since the circular fractal model is both geometrical and analytical, it enables a choice and a proper calibration of the software. The most consistent measurements of the D_0 and D_1 were produced by the software Benoit 3.1.

The application of the cut-off D_0 values to the re-stratification of carcinomas eliminates both the subjectivity and inaccuracy. In consequence, carcinomas can be re-stratified to the seven classes of complexity C1, C2, C3, C4, C5, C6, and C7 (Table 2). In the case of this analysis, the re-stratification was done in about 50% of carcinomas.

The complexity classes are unequivocally defined by the cut-off D_0 values. Those classes contain prostate carcinomas with the similar values of the dimension D_0. As expected, each complexity class contains elements of the corresponding structural Gleason class and a number of carcinomas classified subjectively to the other structural Gleason classes that have the similar D_0-values. Figure 3 presents each carcinoma of the set as a point on the 3D-scatter plot with D_0, D_1, and D_2 as variables. Table 2 summarizes results of the ROC analysis of the re-stratified set.

Class of Equivalence	Sensitivity	Specificity	D_0	AUC	p-value
C1 vs C2	1.00	1.00	1.5450	1.00	< 0.0001
C2 vs C3	1.00	1.00	1.5820	1.00	< 0.0001
C3 vs C4	1.00	1.00	1.6270	1.00	< 0.0001
C4 vs C5	1.00	1.00	1.6490	1.00	< 0.0001
C5 vs C6	1.00	1.00	1.6980	1.00	< 0.0001
C6 vs C7	1.00	1.00	1.7640	1.00	< 0.0001

Table 2. A summary of the ROC analysis for the set of 173 prostate carcinomas characterized by the global fractal dimensions D_0, D_1, and D_2 and re-stratified into the complexity classes as shown in Figure 3. The D_0-cut-off values define the limits between the classes.

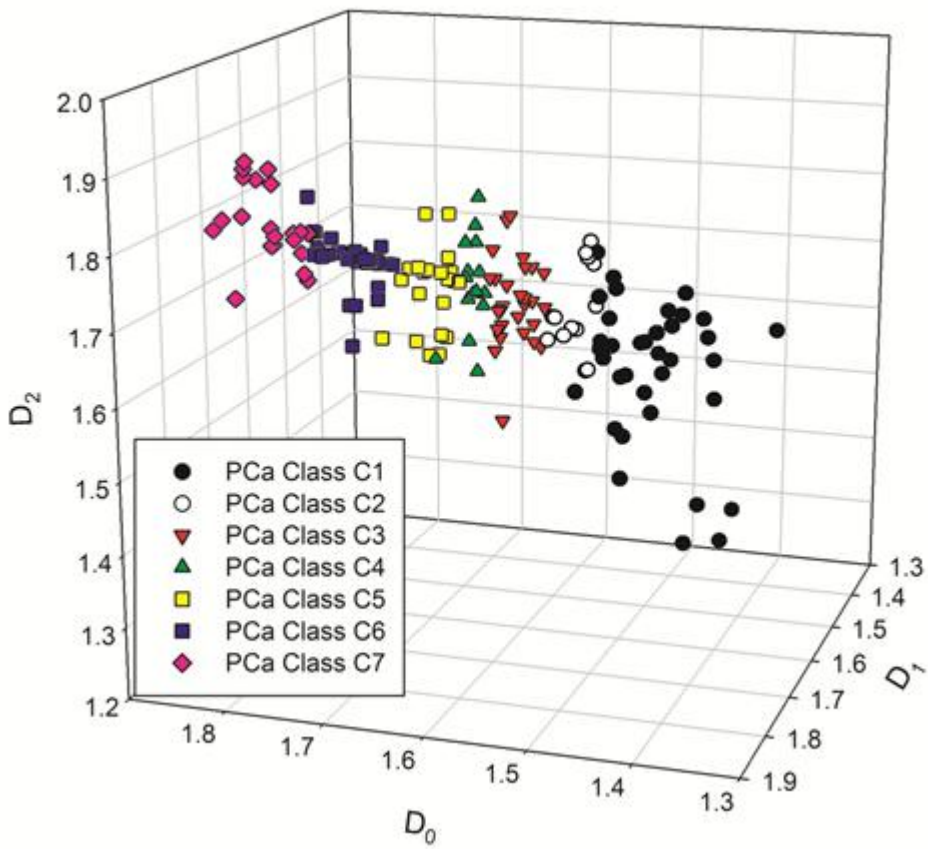

Figure 3. Prostate carcinomas (PCa) were re-stratified into the classes of equivalence called the complexity classes. Those classes are defined by the mean values of the global capacity fractal dimension D_0.There are seven classes of equivalence. Those classes were constructed using a method of the re-stratification. It was done under the following condition: the parameters of the ROC analysis, i.e., area under curve, sensitivity and specificity had to be equal 1.0 (see Table 2). The classes C1, C4, and C7 contain carcinomas with the Gleason score $3 + 3$, $4 + 4$, and $5 + 5$ and with relatively homogeneous tissue architecture as described above in Section 2.

4. The Bekenstein Bound, topology of the circular fractals and tumor aggressiveness. A comparison of the images presented in Figure 1D, 1E, and 1F suggests the existence of a significant difference in complexity between the interacting dynamic cellular systems represented by the circular fractal CF(3) and those represented by the fractals CF$(6 + 0)$ and CF$(6 + 1)$. It should be noticed that the patterns of growth depicted by those fractals represent some consecutive stages in natural history of prostate adenocarcinomas. Those stages are characterized by a loss of the regular spatial glandular architecture in the course of time. Those spatial patterns develop as a result of

dynamic interactions at a variety of levels including the quantum one that determine the localization of cells in spacetime. In this sense, histological images of carcinomas are spatial imprints of the spatio-temporal phenomenon. The spacetime, in which growth and self-organization of dynamic cellular systems occur, is a fragment of the physical spacetime restricted by the principle of unitarity that ensures the sum of probabilities of all possible outcomes of any event during the temporal evolution of the physical system up to the quantum level is always 1. One of the consequences of unitarity is the Bekenstein Bound. That Bound imposes a limit on the amount of information present in any physical system including dynamic cellular systems interacting in the fractal spacetime [2]. Using mass energy equivalence, the Bekenstein Bound is given by the equation

$$I \leq \frac{2\pi cRm}{h \ln 2} \approx 2.577 \cdot 10^{43} Rm \tag{1}$$

in which I is the information expressed in number of bits contained in the quantum states of any physical system limited by the sphere of the radius R measured in meters, with a mass m in kg. The $\ln 2$ factor comes from defining the information as the logarithm to the base 2 of the number of quantum states, h is the reduced Planck constant, c stands for the speed of light.

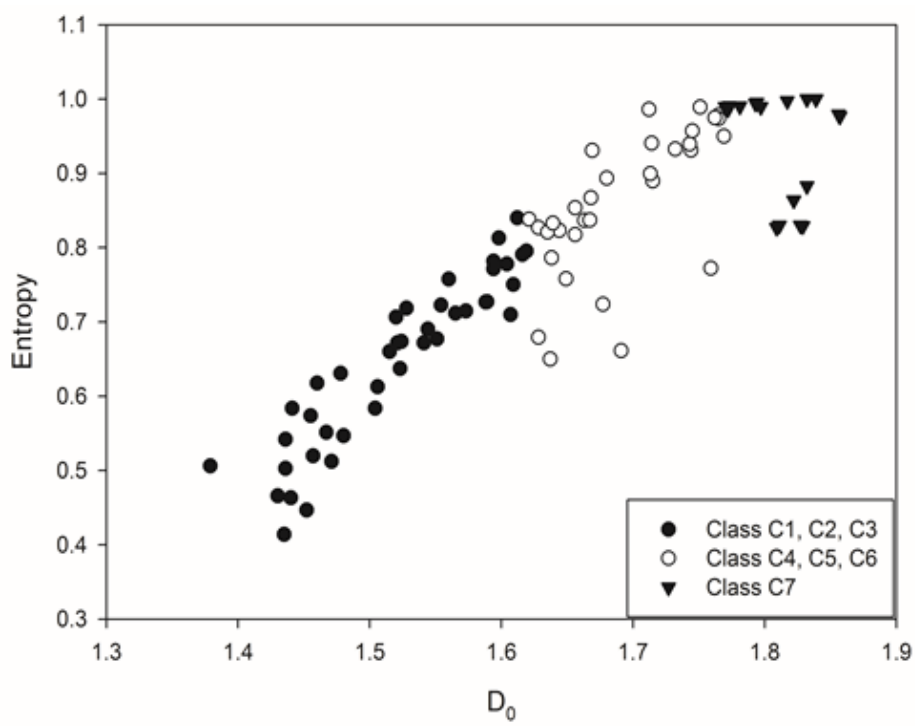

Figure 4. A distribution of entropy as a function of the global fractal dimension D_0 in the subset of prostate carcinomas representing all complexity classes. The function has an algebraic form of the linear function $S = 1.14 \cdot D_0 - 1.08$, in which S denotes entropy. The correlation coefficient is 0.904. The obtained values of the Shannon entropy correspond well with the predictions of the model and re-stratification in the complexity classes.

If we imagine that those three cellular systems are immersed in the equal unit spheres, then either volume or mass of the entire tissue comprising both malignant epithelial cells and normal mesenchymal cells of stroma is approximately the same. However, if we consider only the network of malignant cells, it is clear that complexity of the systems represented by the circular fractals CF(6 + 0) and CF(6 + 1) is higher than in the case of the system represented by the CF(3). Since the only difference between them is a number of cells of approximately similar size (compare Figure 1), then the ratio of the amount of information in the fractal cellular systems represented by the CF(3), CF(6 + 0), and CF(6 + 1) is like 1 : 1.94 : 2.64. This ratio is similar to the ratio of entropy measured for the complexity classes C1, C4 or C7. Both increase almost linearly. Figure 4 shows a distribution of entropy in the subset of prostate carcinomas representing all classes of equivalence.

It should be noticed that the circular fractals in Figure 1 belong to a class of self-affine fractals. Their topology can also be described with a finite amount of information. In particular, the fractals CF(6+0) and CF(6+1) possess the identical topology. Indeed, if

$$f_j(x) = A(x + y_j) \tag{2}$$

for $j = 1, \ldots, m$, map the entire circular fractal F to F_i and $f_i^{-1} f_j(F)$ to F_j, where $F_i \cup F_j \neq \varnothing$, then all neighbor contracting maps are translations [22, 1].

For the hexagasket shown in Figure 1E, the mappings are given by the equation

$$f_j(z) = \frac{1}{3}(z + 2b^j) \tag{3}$$

for $j = 0, 1, \ldots, 5$; $b = \exp i\pi/3$.

In the case of the septagasket presented in Figure 1F, the basic structure of the neighbor graphs do not change, however, a few more labels must be added. Thus, topology of both gaskets remains identical. This finding suggests that the corresponding cellular systems in carcinomas of the complexity class C4 up to C7 may also originate from the same or very similar dynamics generated by the same dynamic forces, despite the fact that there are some structural differences between those carcinomas. In particular, carcinomas of the class C4 form still some very small clusters of malignant cells called pseudoglands. Carcinomas of the class C7 have cellular infiltrates without any gland architecture. It might be expected that the difference in metastatic potential of malignant cells present in both kinds of carcinomas is not so large. Therefore, carcinomas of the class C4 up to C7 might be classified by pathologists to a single category of high-grade carcinomas with the increased risk of metastasis formation. This information denotes that urologists may expect an aggressive course of the disease, and, therefore, the particular cancer patient must be treated aggressively and without a delay from the very beginning. Topology of the fractal CF(3) or CF(4) is different. Those fractals have also lower amount of missing information, and, therefore, are less complex. Those features correlate well with a relatively slow dynamics of the disease. Carcinomas of the classes C1, C2, or C3 might be good candidates for the program of active surveillance, and do not need to be treated immediately.

5. Conclusion. Both a proper risk assessment and a choice of the best strategy in treatment of prostate carcinomas are hot topics in tumor pathology or oncological urology since many years. Results of this study suggest that the detailed classification of prostate carcinomas based on their glandular architecture is too complicated. Human eye and mind are not able to evaluate in an accurate manner many differences in details between different carcinomas, what is a main source of a high inter- and intraobserver variability. Therefore, this classification should be simplified. The results indicate that this simplification is possible, and will offer a better clinical stratification of patients.

First, the circular fractal model of adenocarcinomas that is both geometrical and analytical can be used to select and calibrate the best software for the image analysis.

Second, the complexity measures of the spatial distribution of cancer cell nuclei allow the objective classification of the carcinoma cases in the classes of equivalence. Third, the mean value of the global capacity fractal dimension D_0 defines a limit between those prostate carcinomas that may be followed up without a need for the aggressive treatment, and those high-risk carcinomas that must be treated immediately. This value is 1.5820.

Third, the circular fractal model has been validated in this study by using a large set of prostate carcinomas. The complexity classes based on that model have a limited amount of information. Their complexity changes in a linear manner as shown by the changes of entropy S in a linear function of the D_0 with the coefficient of correlation 0.904. The values of entropy S determine the direction of the natural course of disease. Also, this validates the model in the independent way.

Fourth, the model is of universal nature, and can be applied to stratify any cancer with glandular structure. Geometry of the spatial distribution of cancer cell nuclei in adenocarcinomas growing in different organs can have similar values of fractal dimensions, e.g., prostate, stomach, colon or thyroid carcinomas. Yet, the course of those diseases is very different. Apparently, biological tumor aggressiveness is not the only factor that determines biology of adenocarcinomas.

References

[1] Ch. Bandt, M. Messing, *Self-affine fractals of finite type*, in: Convex and Fractal Geometry, Banach Center Publ. 84, Polish Acad. Sci. Inst. Math., Warsaw 2009, 131–148.

[2] J. D. Bekenstein, *Universal upper bound on the entropy-to-energy ratio for bounded systems*, Phys. Rev. D 23 (1981), 287–298.

[3] M. F. Berger, M. S. Lawrence, F. Demichelis et al., *The genomic complexity of primary human prostate cancer*, Nature 470 (2011), 214–220.

[4] E. D. Crawford, M. C. Scholz, A. J. Kar et al., *Cell cycle progression score and treatment decisions in prostate cancer: results from an ongoing registry*, Current Medical Research and Opinion 30 (2014), 1025–1031.

[5] G. R. Cunha, S. W. Hayward, Y. Z. Wang, W. A. Ricke, *Role of the stromal microenvironment in carcinogenesis of the prostate*, Internat. J. Cancer 107 (2003), 1–10.

[6] J. I. Epstein, *An update of the Gleason grading system*, J. Urology 183 (2010), 433–440.

[7] J. I. Epstein, W. C. Allsbrook, M. B. Amin et al., *The 2005 International Society of Urological Pathology (ISUP) Consensus Conference on Grading of Prostatic Carcinoma*, Amer. J. Surgical Pathology 29 (2005), 1228–1242.

[8] W. A. Gardner Jr., *Histologic grading of prostate cancer: a retrospective and prospective overview*, Prostate 3 (1982), 555–561.

[9] D. F. Gleason, *Classification of prostatic carcinoma*, Cancer Chemotherapy Reports 50 (1966), 125–128.

[10] M. K. Gospodarowicz, D. E. Henson, R. V. P. Hutter, B. O'Sullivan, L. H. Sobin, Ch. Wittekind, *Prognostic Factors in Cancer*, second ed., Wiley-Liss, New York 2001.

[11] C. M. Grant, N. Kyprianou, *Epithelial mesenchymal transition (EMT) in prostate growth and tumor progression*, Translational Andrology and Urology 2 (2013), 202–211.

[12] P. A. Humphrey, *Grading of prostatic carcinoma*, in: Prostate Pathology, ASCP Press, Chicago 2003, 338–374 (Chapter 15).

[13] M. W. Kattan, J. A. Eastham, T. M. Wheeler et al., *Counseling men with prostate cancer: A nomogram for predicting the presence of small moderately differentiated, confined tumors*, J. Urology 170 (2003), 1792–1797.

[14] E. A. Klein, M. R. Cooperberg, C. Magi-Galluzzi et al., *A 17-gene assay to predict prostate cancer aggressiveness in the context of Gleason grade heterogeneity, tumor multifocality, and biopsy undersampling*, European Urology 66 (2014), 550–560.

[15] S. Lamouille, D. Subramanyam, R. Blelloch, R. Derynck, *Regulation of epithelial-mesenchymal and mesenchymal-epithelial transitions by microRNAs*, Current Opinion in Cell Biology 25 (2013), 200–207.

[16] P. C. Lin, E. G. Giannopoulou, K. Park et al., *Epigenomic alterations in localized and advanced prostate cancer*, Neoplasia 15 (2013), 373–383.

[17] J. E. McDunn, Z. Li, K. P. Adam et al., *Metabolomic signatures of aggressive prostate cancer*, Prostate 73 (2013), 1547–1560.

[18] G. T. Mellinger, D. F. Gleason, J. Bailar III, *The histology and prognosis of prostatic cancer*, J. Urology 97 (1967), 331–337.

[19] R. Montironi, A. Lopez-Beltran, L. Cheng, F. Montorsi, M. Scarpelli, *Central prostate pathology review: should it be mandatory?*, European Urology 64 (2013), 199–203.

[20] P. L. Nguyen, D. Schultz, A. A. Renshaw et al., *The impact of pathology review on treatment recommendations for patients with adenocarcinoma of the prostate*, Urologic Oncology – Seminars and Original Investigations 22 (2004), 295–299.

[21] E. Pin, C. Fredolini, E. F. Petricoin, *The role of proteomics in prostate cancer research: biomarker discovery and validation*, Clin. Biochem. 46 (2013), 524–538.

[22] R. S. Strichartz, *Isoperimetric estimates on Sierpinski gasket type fractals*, Trans. Amer. Math. Soc. 351 (1999), 1705–1752.

[23] B. Turkbey, P. L. Choyke, *Multiparametric MRI and prostate cancer diagnosis and risk stratification*, Current Opinion in Urology 22 (2012), 310–315.

[24] P. Waliszewski, *A principle of fractal-stochastic dualism and Gompertzian dynamics of growth and self-organization*, Biosystems 82 (2005), 61–73.

[25] P. Waliszewski, *Towards the objective grading of prostate carcinomas*, in: Fractals and Complexity, ed. P. Waliszewski, FA Format, Wrocław 2013, 16–23, ISBN 978-83-936598-0-7.

[26] P. Waliszewski, J. Konarski, *On time-space of nonlinear phenomena with Gompertzian dynamics*, Biosystems 80 (2005), 91–97.

[27] P. Waliszewski, F. Wagenlehner, S. Kribus, W. Schafhauser, W. Weidner, S. Gattenlöhner, *Objektivierung des Tumorgradings bei Prostatakarzinomen anhand der globalen und lokalen fraktalen Dimensionen: Gleason* $3+4=7a \neq$ *Gleason* $4+3=7b$. *Objective grading of prostate carcinoma based on fractal dimensions: Gleason* $3+4=7a \neq$ *Gleason* $4+3=7b$, Urologe A 53 (2014), 1504–1511.